

# Two Are Better Than One: A Design Principle for Ultralong-Persistent Luminescence of Pure Organics

Parvej Alam, Nelson L. C. Leung, Junkai Liu, Tsz Shing Cheung, Xuepeng Zhang, Zikai He, Ryan T. K. Kwok, Jacky W. Y. Lam, Herman H. Y. Sung, Ian D. Williams, Christopher C. S. Chan, Kam Sing Wong, Qian Peng, and Ben Zhong Tang\*

Because of their innate ability to store and then release energy, long-persistent luminescence (LPL) materials have garnered strong research interest in a wide range of multidisciplinary fields, such as biomedical sciences, theranostics, and photonic devices. Although many inorganic LPL systems with afterglow durations of up to hours and days have been reported, organic systems have had difficulties reaching similar timescales. In this work, a design principle based on the successes of inorganic systems to produce an organic LPL (OLPL) system through the use of a strong organic electron trap is proposed. The resulting system generates detectable afterglow for up to 7 h, significantly longer than any other reported OLPL system. The design strategy demonstrates an easy methodology to develop organic long-persistent phosphors, opening the door to new OLPL materials.


Long-persistent luminescent<sup>[1,2]</sup> (LPL) materials have demonstrated great potential and performance in multiple areas, such as life sciences,<sup>[3]</sup> the biomedical field,<sup>[2,4]</sup> and photovoltaics,<sup>[5]</sup> as they offer fascinating possibilities for their ability to store and slowly release excited state energy. For example in biomedical applications, LPL materials can be used postexcitation, overcoming any issue of autofluorescence.<sup>[6–8]</sup> Currently, the most successful LPL materials make use of transition and rare-earth metal ions.<sup>[9,10]</sup> Although the metals grant exceptionally long afterglows that range from minutes to hours, with some systems lasting days and weeks,<sup>[11]</sup> they are not without their inherent

drawbacks. In addition to the higher material costs of these rare-earth metals, many inorganic LPLs require harsh synthetic procedures,<sup>[11]</sup> further increasing research costs. Organic LPL (OLPL) materials,<sup>[12–16]</sup> offer the promise of a multitude of benefits: easier synthesis, easier modification for targeted functionality, and easier processing. However, the development of OLPL materials has encountered many obstacles. To access long lived states in organic compounds, there have been many designs to exploit the excited triplet state. Though access to and from the triplet state is a forbidden process and once thought to be too inefficient for effective use at room temperature,<sup>[17]</sup> recent

advances have vastly increased intersystem crossing efficiency by enhancing spin–orbit coupling (SOC) with the use of heteroatoms,<sup>[18,19]</sup> the carbonyl functional group,<sup>[20–22]</sup> heavy atom effects,<sup>[23–27]</sup> and multimer-enhanced intersystem crossing.<sup>[28–32]</sup> Equally important is protecting the long-lived triplet after its generation, due to the fact that they are particularly sensitive to molecular vibrational quenching and atmospheric oxygen. In this regard, recent works have accomplished this through the use of crystals,<sup>[33,34]</sup> metal–organic frameworks,<sup>[35]</sup> H-aggregation,<sup>[36]</sup> and others.<sup>[30,32,37]</sup> Although there have been many achievements in generating organic room-temperature

Dr. P. Alam, Dr. N. L. C. Leung, J. Liu, T. S. Cheung, Dr. X. Zhang, Dr. R. T. K. Kwok, Dr. J. W. Y. Lam, Dr. H. H. Y. Sung, Prof. I. D. Williams, Prof. B. Z. Tang  
Department of Chemistry  
Hong Kong Branch of Chinese National Engineering Research Center for Tissue Restoration and Reconstruction  
Department of Chemical and Biological Engineering  
The Hong Kong University of Science and Technology  
Clear Water Bay, Kowloon, Hong Kong 999077, China  
E-mail: tangbenz@ust.hk

Prof. Z. He  
School of Science  
Harbin Institute of Technology, Shenzhen  
HIT Campus of University Town  
Shenzhen 518055, China

 The ORCID identification number(s) for the author(s) of this article can be found under <https://doi.org/10.1002/adma.202001026>.

DOI: 10.1002/adma.202001026

Dr. C. C. S. Chan, Prof. K. S. Wong  
Department of Physics  
The Hong Kong University of Science and Technology  
Clear Water Bay, Kowloon, Hong Kong 999077, China

Prof. Q. Peng  
Key Laboratory of Organic Solids  
Beijing National Laboratory for Molecular Sciences  
Institute of Chemistry  
Chinese Academy of Sciences  
Beijing 100190, China

Prof. B. Z. Tang  
Center for Aggregation-Induced Emission  
SCUT-HKUST Joint Research Institute  
State Key Laboratory of Luminescent Materials and Devices  
South China University of Technology  
Guangzhou 510640, China

Prof. B. Z. Tang  
HKUST-Shenzhen Research Institute  
No. 9 Yuexing 1st RD, South Area, Hi-tech Park, Nanshan  
Shenzhen 518057, China

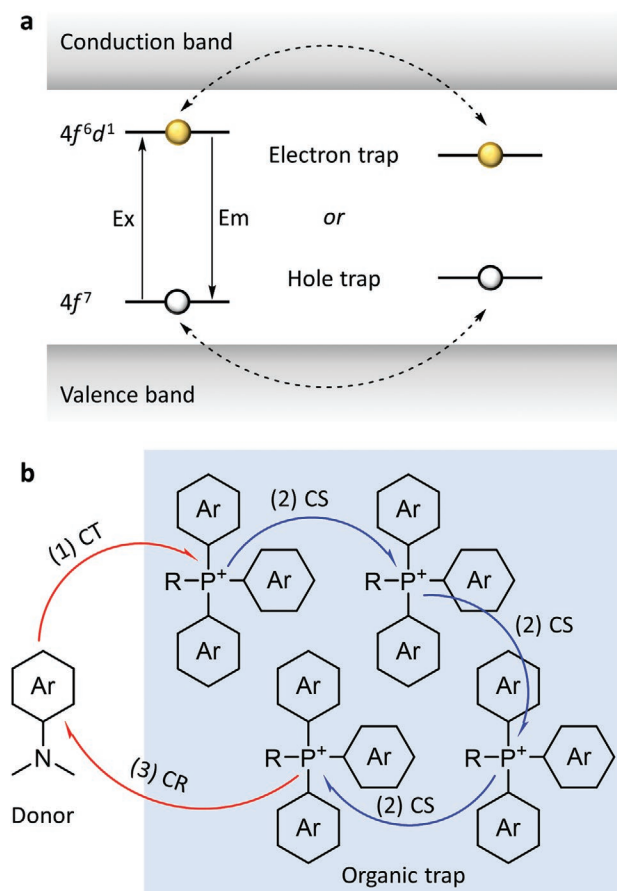


**Figure 1.** Schematic representations of mechanisms behind inorganic and organic persistent luminescence. a) Inorganic long-persistent luminescence can be achieved through electron or hole trap mechanisms. In the electron trap, it is proposed after excitation (Ex), the excited electron travels through the conduction band to an electron accepting trap. In the hole trap, an electron fills the hole by traveling through the valence band. In both cases, relaxation becomes blocked, either because the excited electron has migrated away, or the hole has become filled. Thermal disturbances restore the electron or hole, producing afterglow emission (Em). b) A proposed mechanism for organic long-persistent luminescence where a cationic quaternary phosphonium core acts as an organic trap and an aromatic amine as an electron donor. First 1) photoinduced charge transfer (CT) occurs between the donor and acceptor molecules followed by 2) charge separation (CS). Multiple CS can occur before the final step 3), charge recombination (CR), resulting in OLPL.

phosphorescent systems,<sup>[31,37–45]</sup> their lifetimes cannot match the durations of inorganic LPL materials.

By applying concepts from the mechanistic understand of inorganic LPL systems to OLPLs, it can be possible to merge the diverse benefits of organic systems with the performance of inorganics. One of the most successful methods to achieve LPL in inorganic systems is through the use of traps (Figure 1a), which allow for energy storage and its subsequent slow release via thermal disturbances. Inspired by the role of inorganic trap species, we hypothesized a purely organic biontentic system, a system made of two parts, i.e., i) an emitter and ii) a trap (Figure 1b). Just as the heavy metals store charge carriers and slowly release them back into the system for eventual emission, organic molecules could theoretically do the same thing.

To test our mechanistic principle, we first set out to find an ionic core system that could work as a strong electron acceptor. In our search, we discovered, synthesized, and characterized (Figures S1–S5, Supporting Information) a series of pure organic quaternary phosphonium bromide salts, TPP-3CB, TPP-4CB, TPP-3C2B, and TPP-4C2B, which exhibit observable afterglow (Figure 2; and Videos S1–S4, Supporting Information). These four compounds were purified and recrystallized several times before characterization, with the ionic nature of the compounds aiding the formation of the crystal growth. Their crystal structures displayed a distorted tetrahedral geometry ( $108.7^{\circ}$ – $110.8^{\circ}$ ) and the distance between the phosphonium and bromide ions were measured to be in the range of 4.50–4.75 Å (Figure S6, Supporting Information). In all four phosphonium salts, none of them exhibit  $\pi$ – $\pi$  interactions or anionic bromide– $\pi$  interactions; examining their packing (Figure S7, Supporting Information) only C–H $\cdots\pi$  and C–H $\cdots$ Br interactions exist (Table S1, Supporting Information). These interactions, as well as electrostatic interactions work together to suppress molecular motion in the crystal enhancing phosphorescence efficiency. The absorption spectra of TPP-3CB, TPP-4CB, TPP-3C2B, and TPP-4C2B were recorded in dilute acetonitrile solutions ( $10 \times 10^{-6}$  M), and they showed similar absorption bands at 265, 268, and 275 nm which were attributed to  $\pi$ – $\pi^*$  transitions from the phenyl moieties of the phosphonium core (Figure S8, Supporting Information).

The crystals of all four phosphonium bromide salts showed an emission maximum of 480 nm (Figure 2b), and surprisingly, their excitation spectra (Figure S9, Supporting Information) at 480 nm emission revealed a maximum excitation band at 310 nm which was attributed to a photoinduced charge transfer from the bromide counterion to the phosphonium core. Thus, subsequent PL and lifetime measurements of TPP-3CB, TPP-4CB, TPP-3C2B, and TPP-4C2B crystals were recorded by 310 nm excitation. From the time-resolved PL decay curves (Figure 2c), the average lifetimes of TPP-3CB, TPP-4CB, TPP-3C2B, and TPP-4C2B crystals at 480 nm measured at room temperature (298 K) were 157, 200, 159, and 164 ms, respectively, indicating the ultralong afterglow nature of these materials and the average lifetimes of these phosphonium salts measured at 77 K in dilute solution were found to be 632, 410, 320, and 717 ms, respectively (Figures S10–S13, Supporting Information). Under 254 nm handheld UV lamp excitation, intense greenish blue emission could be observed from the crystals (Figure 2d).

We further took the crystal of TPP-3CB as a target model and employed combined quantum mechanics and molecular mechanics method (QM/MM) to simulate the photophysical process in the crystal, optimizing the excited singlet ( $S_1$ ) and triplet ( $T_1$ ) states and their molecular orbitals furnished by the ONIOM method (Figure 3a–c, and Figure S14, Supporting Information). At the  $S_1$  geometry (Figure 3a), the molecular orbitals of the  $S_1$  and  $T_1$  of TPP-3CB (Figure S15, Supporting Information) show complete charge transfer from its bromide anion to the phosphonium cation, furnishing excited radical pairs. Initially, a large separation of the orbitals involved in the transition from  $S_0$  to  $S_1$  resulted in a small exchange energy from  $S_1$  to  $T_1$  state, producing an energy gap between  $S_1$  and  $T_1$  that is smaller than 0.1 eV facilitating intersystem crossing. Furthermore, the bromide anion endows the transition process

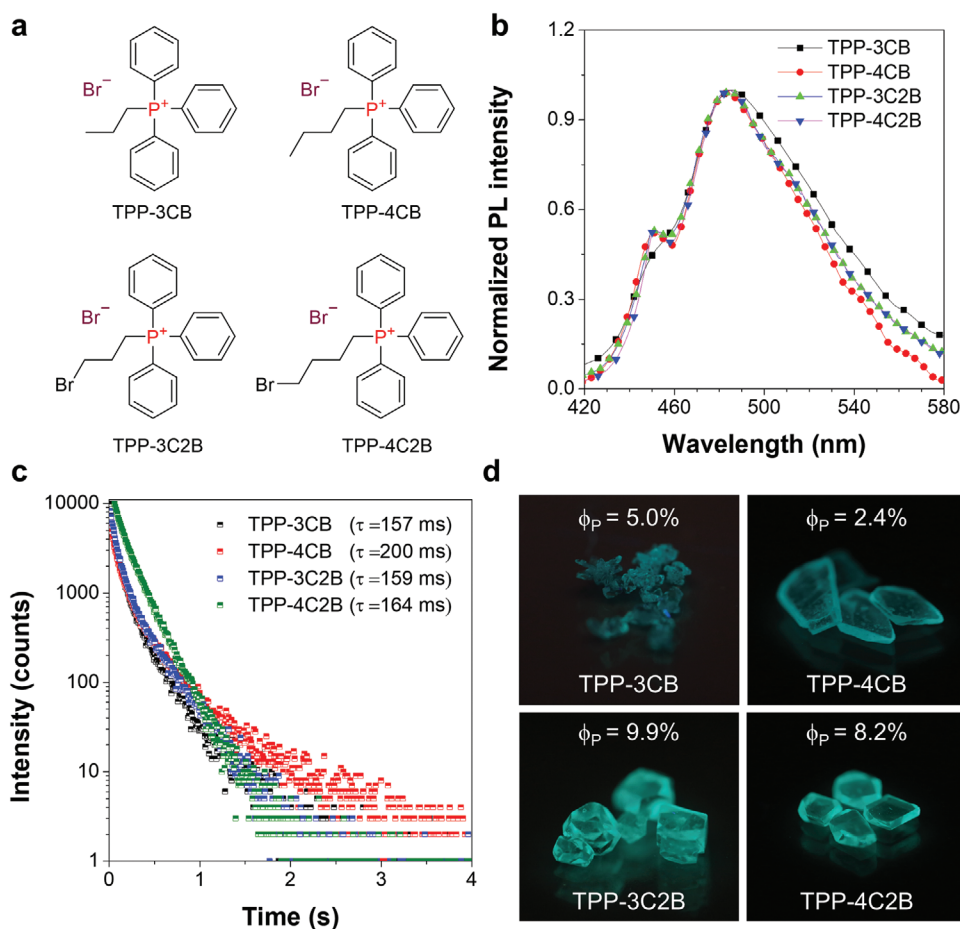


**Figure 2.** a) Chemical structures, b) PL spectra, and c) time-resolved PL decay (at 480 nm) of crystalline powders of TPP-3CB, TPP-4CB, TPP-3C2B, and TPP-4C2B at 298 K;  $\lambda_{\text{ex}} = 310$  nm. d) Photographs of TPP-3CB, TPP-4CB, TPP-3C2B, and TPP-4C2B under UV excitation at 254 nm as well as their phosphorescence quantum yields ( $\Phi_p$ ).

with a spin-orbit coupling constant as large as  $327.39 \text{ cm}^{-1}$ , which further enhances the transition between the  $S_1$  and  $T_1$  state.

As such, both the complete charge-transfer characteristic and the strong SOC provides a firm foundation for the spin-orbit charge transfer (SOCT)<sup>[46]</sup> intersystem crossing process from  $S_1$  to  $T_1$  for the phosphonium bromide complex. In addition, the excited state radical pair is also susceptible to hyperfine coupling (HFC)<sup>[47]</sup> effects which provide another channel for intersystem crossing;<sup>[48]</sup> as the radicals are located on two separate locations, they experience different local magnetic fields leading to spin-mixing where rephasing (Figure 3e) and spin-flipping transitions facilitate intersystem crossing. In this way, upon excitation the molecule initially becomes an excited singlet radical pair ( $^1\text{RP}$ ), but due to SOCT and HFC effects, not only does the  $^1\text{RP}$  easily intersystem cross to become an excited triplet radical pair ( $^3\text{RP}$ ), the  $^3\text{RP}$  can also easily intersystem cross back into the  $^1\text{RP}$  (Figure 3d,e). According to the calculations, the RP state changes when the molecule relaxes to its  $T_1$  geometry, that is, at the optimized  $T_1$  geometry, charge-transfer/radical pair nature is lost. The molecular orbitals indicate at the  $T_1$  minimum, the exciton is localized on the phosphonium core (Figure 3c) indicative of a second charge transfer event. The  $T_1$

becomes energetically separated from the  $S_1$  with an energy difference of 0.957 eV thus trapping the excited state for room-temperature phosphorescence.

Considering that it has been reported that excited-state charge separation (CS) can be beneficial for OLPLs<sup>[13]</sup> and, taking cues from inorganic LPL systems, if we introduce moieties to “trap” charge carriers, it may be possible to further extend the afterglow duration. This could be made achieved by using a strong electron accepting molecule as the bulk. In other words, the bulk acts as one large “trap” slowing down recombination. To verify our hypothesis, we attempted to develop a biontic OLPL system using a phosphonium bromide salt as a strong electron acceptor (lowest unoccupied molecular orbital (LUMO) =  $-1.1$  eV; Figure S16, Supporting Information), which would act as the organic trap, and *N,N*-dimethylaniline (DMA) as an electron donor (highest occupied molecular orbital (HOMO) =  $-5.2$  eV; Figure S16, Supporting Information). We were able to dope DMA into TPP-3C2B by first mixing DMA with a dichloromethane (DCM) solution of TPP-3C2B and then allowing crystals to grow. These crystals exhibited a strong emission at 500 upon 365 nm excitation (Figure 4a). For reference, the absorption spectrum of DMA in acetonitrile has two bands

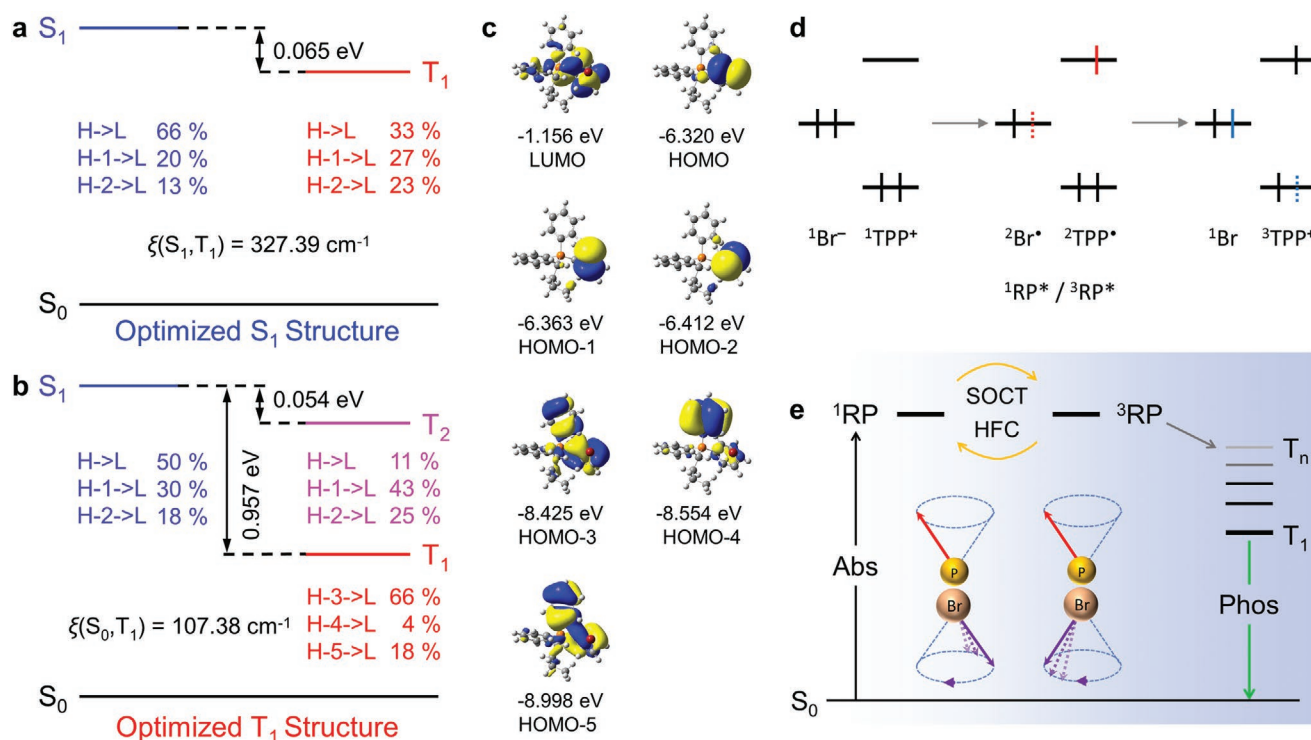


**Figure 3.** QM/MM calculations at TD-DFT level of the singlet and triplet excited states. a,b) The TPP-3CB crystal structure was used to obtain an optimized geometry for the  $S_1$  (a) and  $T_1$  (b) excited states surrounded by 43 molecules. c) Molecular orbitals calculated from the optimized  $T_1$  structure. d) Schematic representation of electrons in TPP-3CB starting from the ground state, after the first charge transfer excitation (colored in red) into the radical pair (RP), and the second charge transfer event (colored in blue) into the  $T_1$  state. e) Modified Jablonski diagram showing the formation of the singlet radical pair ( $^1\text{RP}$ ) after absorption (Abs). Spin-orbit charge transfer (SOCT) and hyperfine coupling (HFC) can aid in the interconversion between the  $^1\text{RP}$  and the triplet radical pair ( $^3\text{RP}$ ) as illustrated by the rephasing of the radical pair electrons in separate locations. The RP then relaxes into the  $T_1$  state before phosphorescence is observed.

at 252 and 300 nm (Figure S17, Supporting Information) and has an emission band at 350 nm. Since neither DMA nor TPP-3C2B have absorption bands at 365 nm (Figure S18, Supporting Information), this suggests the excitation of the TPP-3C2B:DMA crystals has photoinduced charge-transfer characteristics. Furthermore, the emission band of TPP-3C2B:DMA at 500 is  $\approx 20$  nm redshifted from TPP-3C2B, suggesting an exciplex emission (Figure S19, Supporting Information). The 2D excitation and emission maps of TPP-3C2B:DMA (Figure S20a, Supporting Information), TPP-3C2B (Figure S20b, Supporting Information), and DMA (Figure S20c,d, Supporting Information) further aid in the visualization. Pure DMA and TPP-3C2B show highly different maps when compared to TPP-3C2B:DMA. Specifically, at 365 nm excitation, neither TPP-3C2B nor DMA exhibit any detectable emission. In addition, the high-performance liquid chromatography (HPLC) data (Figure S21, Supporting Information) confirm the presence of DMA in the TPP-3C2B:DMA samples. Furthermore, transient absorption spectroscopy of TPP-3C2B:DMA was also performed to further investigate its properties. The spectrum showed the formation of a new band at 475 nm (Figure S22a, Supporting Information). Since, this band matches well with the absorption of the  $\text{DMA}^{\cdot+}$  produced in situ in the presence of  $\text{Cu}(\text{ClO}_4)_2$  (Figure S22b, Supporting Information),<sup>[49]</sup> it suggests the presence of radical or CS after UV excitation. In addition, the presence of CS was verified using electron spin resonance

(ESR) measurement of the OLPL system. The presence of a strong ESR signal after UV radiation was attributed to formation of radical (Figure S23, Supporting Information). In summary, after 60 s of 365 nm UV excitation, there is evidence that long-lived charge-separated states could be generated, resulting in emission that could be detected for up to 7 h (Figure 4; and Video S5, Supporting Information) at ambient conditions. We attempted to dope DMA into the other phosphonium bromide salts, but LPL was not observed in these systems.

Examining the emission decay profile under logarithmic x- and y-axes (Figure S24, Supporting Information), the profile matches a power decay which Hamill termed as Debye–Edwards law,<sup>[50]</sup> where PL intensity  $\propto t^{-m}$ . The Debye–Edwards law describes electron recombination kinetics where after excitation electrons become trapped in rigid media and slowly recombine with positive holes. The index  $m$  reflects the rate of recombination and can have a numerical value from 0.1 to 2.0. The larger the  $m$ -value, the faster the decay. Typically, the exponent  $m$  has a value  $\approx 1$ .<sup>[9,13,50]</sup> In our system, fitting with the Debye–Edwards law exhibited changes depending on the amount of time that had passed. After 12 min of stabilization, the  $m$ -value of the system had a fitted value of 1.009 from 12 min to 3.4 h and in the last 3.4 to 7 h, the  $m$ -value decreased to 0.663. The decrease from 1.009 to 0.663 at the end is quite easily understood: near the end, the population of both electrons and holes dwindle and as such recombination becomes less probable decreasing



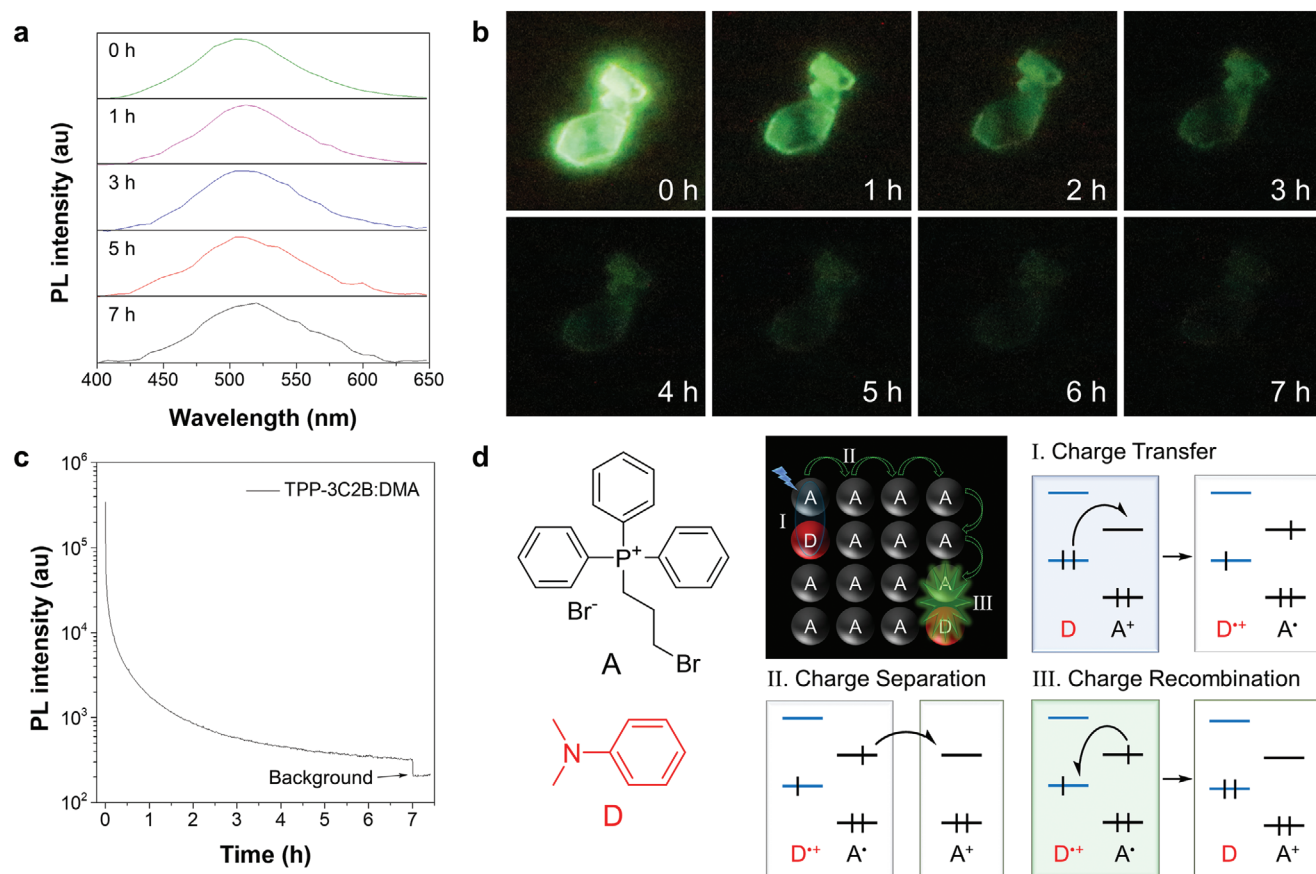


**Figure 4.** Chemical structure and photophysical properties of TPP-3C2B:DMA. a) Emission spectra of TPP-3C2B:DMA crystals measured at different times (0–7 h) after the cessation of excitation at 365 nm. b) Photographs of TPP-3C2B:DMA crystals taken under 365 nm UV excitation and its subsequent afterglow. c) Afterglow kinetic measurement of PL intensity at 500 nm over 7 h. After 7 h, the sample was removed to reveal background level measurement. d) Left: chemical structures of TPP-3C2B labeled A for acceptor, and *N,N*-dimethylaniline (DMA) labeled D for donor. Right: scheme representing the formation of the radical pair through charge transfer, subsequent CS and finally charge recombination to achieve long-persistent luminescence.

the recombination rate. The fitting further supports a charge transfer event and subsequent charge recombination process in the OLPL crystal. The obtained nonexponential decay endorses that the long-lasting emission, i.e., LPL, originates from CS states between donor and acceptor molecules.<sup>[51]</sup>

The crystalline nature of TPP-3C2B:DMA protects the photo-generated radicals from atmospheric oxygen and suppresses nonradiative deactivation pathways allowing for such a long afterglow. These crystals exhibit good stability showing no visible changes to its afterglow duration even after being kept for more than 45 days under ambient dark conditions (Video S6, Supporting Information).

The reproducibility of this OLPL system was repeated several times by simply mixing of DMA/TPP-3C2B (10:1 mol ratio) in DCM/EA (1:1 v/v) with varying maximum LPL durations ranging from 1 to 7 h. We have also investigated how the DMA:TPP-3C2B ratio might affect the LPL duration. We grew crystals with 8–36 molar equivalent of DMA to TPP-3C2B (Figure S25, Supporting Information) and all the crystals grown exhibited 7 h of LPL. The crystals grown from 8 and 12 molar equivalent of DMA exhibited slightly weaker emission at 7 h when compared to the 16, 18, and 36 equivalents. The effect, however, does not appear to be particularly strong. We believe a

key factor of the OLPL duration is the amount of DMA trapped inside the crystals. At this point in time, we are further investigating how to control this parameter.

Through careful analysis of the TPP-3C2B:DMA, it becomes possible to draw mechanistic insights to help design OLPL systems with even longer durations. The success of TPP-3C2B gives insight into factors that endow the system with such long-persistent luminescence. One of the most important factors to the extraordinary duration of TPP-3C2B:DMA lies with the organic trap, the bulk crystal TPP-3C2B. Protection of the excited state is of utmost importance to ensuring high efficiency. In this case, the excited radical species, which are inherently reactive, can be easily lost. The phenyl rings decorating the phosphonium core stabilize the radical via steric protection,<sup>[52]</sup> acting as bulky barriers hindering unwanted reactions. In addition, calculations show the radical is able to delocalize among the phenyl rings (Figure S26, Supporting Information) further enhancing its stability.<sup>[52]</sup> The ionic nature of the material also aids in the crystallization, which protects the system from oxygen quenching maximizing emission efficiency. Another important factor that bestows such long durations is the trap's ability to hold onto the electron. The cationic nature of the phosphonium core is an ideal target to accept

the electron of the photoinduced charge transfer process. Furthermore, being surrounded by other cationic phosphoniums, the excited radical can migrate to multiple cores (Figure 4d), before finally recombining with a DMA radical resulting in the observed emission. Stronger, and better designed traps can likely even further increase the time the radical is stored before it jumps to another location. The principles exemplified by the success of TPP-3C2B can be applied to future OLPL systems producing even longer-lived emission and of varied colors and wavelengths. In addition, the OLPL system can be further tuned by modifying the donor molecule. Our group is currently working to develop OLPL systems based on these new insights.

In conclusion, we demonstrate a guiding design principle using strong organic traps to produce OLPL with previously unseen durations. The organic trap stabilizes and protects the excited radical, allowing the system to slowly recombine generating persistent luminescence. In TPP-3C2B:DMA, the cationic triphenylphosphonium core serves as a perfect trap, by first acting as a strong electron acceptor of the photoinduced charge transfer event, and then serving as multiple protective traps before the radical finally migrates back to a DMA for recombination. The insights demonstrated by our investigation will allow the future generation of highly persistent organic luminescent systems that may further propel the development and applications in the fields of medical science and optoelectronic devices.

## Experimental Section

**Materials and Instruments:** Triphenylphosphine, 1-bromopropane, 1-bromobutane, 1,3-dibromopropane, 1,4-dibromobutane, and dimethylaniline were purchased from J&K Scientific. Acetonitrile (HPLC grade) was purchased from Merck. All the molecules synthesized were purified by column chromatography and recrystallized using double layer solution diffusion with dichloromethane/hexane or dichloromethane/ethyl acetate for three times, and fully characterized by <sup>1</sup>H NMR, <sup>13</sup>C NMR, <sup>31</sup>P NMR, and high-resolution mass spectroscopy (HRMS) and elemental analysis. The OLPL crystals, TPP-3C2B:DMA, were grown by first dissolving 100 mg of TPP-3C2B in 5 mL of DCM, followed by the addition of DMA, and finally 5 mL of ethyl acetate was layered on top. <sup>1</sup>H, <sup>13</sup>C, and <sup>31</sup>P NMR spectra were recorded on a Bruker AV 400 Spectrometer at 400, 100, and 160 MHz in CDCl<sub>3</sub>, respectively. Tetramethylsilane was used as the internal standard. High-resolution mass spectra were recorded on a GCT premier CAB048 mass spectrometer operating in MALDI-TOF mode. Elemental analysis was performed on a Thermo Finnigan Flash EA1112. Gel filtration chromatography was performed using a ZORBAX SB-C18 column (Agilent) conjugated to an Agilent 1260 Infinite HPLC system. Before each HPLC run, the sample was purified via 0.22 μm filter to remove any aggregates. The flow rate was fixed at 1.0 mL min<sup>-1</sup>; the injection volume was 100 μL and each sample was run for 10 min. The absorption wavelength used was set at 254 nm. Acetonitrile/water (95:5 v/v) was used as the running solvent system. The photoluminescence/excitation spectra were measured on a PerkinElmer LS 55 spectrophotometer and Horiba Fluoromax 4 spectrofluorometer. Quantum yields of the solids were recorded on Hamamatsu, C13534 at room temperature with a calibrated integrating sphere system. The lifetime was measured on an Edinburgh FLSP 920 fluorescence spectrophotometer equipped with a Xenon arc lamp (Xe900) and a microsecond flash-lamp (uF900). Cyclic voltammetry measurements were recorded on a CHI potentiostat model 604E. The platinum wire and platinum and Ag/AgCl electrodes were used as counter, working, and reference electrodes, respectively, and the scan rate was maintained to 50 mV s<sup>-1</sup>, ESR (JES-FA200) measurements were carried out in presence of UV excitation (λ<sub>ex</sub> = 365 nm). Single crystal

data were collected on a Bruker Smart APEXII CCD diffractometer using graphite monochromated Cu Kα radiation (λ = 1.54 178 Å). The photos and videos were recorded by a Canon EOS 7D Mark II. The photographs for the OLPL were taken with 30 s long exposures on a manual setting with f/2.8 and ISO 16 000 to better capture the emission and were later joined together to form Movies S5 and S6 (Supporting Information).

Average decay lifetimes (τ) were obtained from individual lifetimes τ<sub>i</sub> and amplitudes a<sub>i</sub> of multiexponential evaluation through following Equation 1 and S1 (Supporting Information)

$$\tau = \frac{\sum_i a_i \tau_i^2}{\sum_i a_i \tau_i} \quad (1)$$

**Computational Methods:** To explore room temperature phosphorescence of the quaternary phosphonium salts, theoretical calculations were carried out to draw insight from a quantum mechanical point of view. TPP-3CB was taken as a target compound and built a computational model based on the crystal of TPP-3CB using combined quantum mechanics and molecular mechanics methods (QM/MM). An ONIOM model was constructed by cutting a cluster containing 43 molecules from the single crystal structure (Figure S14, Supporting Information) to calculate the electronic structures at the singlet and triplet excited states using Gaussian 16 package. The central molecule was treated as the QM part at (TD)M06-2X/6-311G(d, p) level and the surrounding molecules acted as the MM part with the universal force field. The central molecule was optimized its S<sub>0</sub>, S<sub>1</sub>, and T<sub>1</sub> geometries while the surrounding molecules were frozen. The analytical frequencies of the S<sub>0</sub>, S<sub>1</sub>, and T<sub>1</sub> were conducted to confirm the structures with lowest energy. The spin-orbit coupling constants between singlet and triplet excited states were calculated using Beijing Density Function (BDF) program with (TD)M06-2X as the function and CC-PVDZ as the basis set.

**General Synthesis Procedure for Alkyl Phosphonium Salts (TPP-3CB and TPP-4CB):** To an oven dried round bottom flask sealed with a rubber stopper, triphenylphosphine (1.6 mmol) and bromoalkanes (1-bromopropane/1-bromobutane, 1.6 mmol) were added, followed by the addition of dry toluene (20 mL) (Scheme S1, Supporting Information). The reaction mixture was refluxed at 120 °C for 12 h. Then, the mixture was evaporated under reduced pressure to afford the crude product which was further purified by column chromatography using methanol/DCM mixture as an eluent to give a solid product in 65–75% yield.

**General Synthesis Procedure for Bromoalkyl Phosphonium Salts (TPP-3C2B and TPP-4C2B):** To an oven dried round bottom flask sealed with rubber stopper, triphenylphosphine (1.6 mmol) and dibromoalkanes (1,3 dibromopropane/1,4 dibromobutane, 1.6 mmol) were added, followed by the addition of dry toluene (20 mL) (Scheme S2, Supporting Information). The reaction mixture was refluxed at 120 °C for 12 h. Then, the mixture evaporated under reduced pressure to afford the crude product which was further purified by column chromatography using methanol/DCM mixture as an eluent to give a solid product in 55–60% yield.

**TPP-3CB:** <sup>1</sup>H NMR (400 MHz, CDCl<sub>3</sub>) δ (ppm): 7.75–7.63 (m, 9H), 7.65–7.53 (m, 6H), 3.73–3.27 (m, 2H), 1.74–1.30 (m, 2H), 1.10 (td, J = 7.3, 1.7 Hz, 3H), <sup>13</sup>C NMR (100 MHz, CDCl<sub>3</sub>) δ (ppm): 134.42, 134.39, 132.93, 132.83, 129.92, 129.80, 117.87, 117.02, 23.99, 23.50, 15.82, 15.78, 14.73, 14.56, <sup>31</sup>P NMR (162 MHz, CDCl<sub>3</sub>) δ (ppm): 23.54, HRMS, m/z: ([M]<sup>+</sup>), calculated 305.1454, found, 305.1492, Elemental Analysis for C<sub>21</sub>H<sub>22</sub>BrP: C (65.47, 65.59), H (5.76, 6.18).

**TPP-4CB:** <sup>1</sup>H NMR (400 MHz, CDCl<sub>3</sub>) δ (ppm): 8.02–7.73 (m, 9H), 7.70–7.50 (m, 6H), 3.67 (ddd, J = 12.7, 10.0, 7.8 Hz, 2H), 1.72–1.23 (m, 4H), 0.85 (t, J = 7.1 Hz, 3H), <sup>13</sup>C NMR (100 MHz, CDCl<sub>3</sub>) δ (ppm): 134.44, 134.41, 132.96, 132.86, 129.95, 129.82, 117.95, 117.09, 23.90, 23.86, 23.13, 22.97, 22.16, 21.66, 13.07. <sup>31</sup>P NMR (162 MHz, CDCl<sub>3</sub>) δ (ppm): 24.38, HRMS, m/z: ([M]<sup>+</sup>), calculated 319.1610, found, 319.1603, Elemental Analysis for C<sub>22</sub>H<sub>24</sub>BrP: C (66.17, 66.59), H (6.06, 6.18).

**TPP-3C2B:** <sup>1</sup>H NMR (400 MHz, CDCl<sub>3</sub>) δ (ppm): 7.87–7.72 (m, 9H), 7.70–7.56 (m, 6H), 4.07–3.90 (m, 2H), 3.79 (td, J = 6.3, 1.2 Hz, 2H), 2.24–2.04 (m, 2H), <sup>13</sup>C NMR (100 MHz, CDCl<sub>3</sub>) δ (ppm): 134.63, 134.60, 133.05, 132.95, 130.03, 129.91, 117.60, 116.74, 32.89, 32.69, 25.57, 21.22, 20.69, <sup>31</sup>P NMR (162 MHz, CDCl<sub>3</sub>) δ (ppm): 23.87, HRMS, m/z: ([M]<sup>+</sup>),

calculated 383.0559, found, 383.0579, Elemental Analysis for C<sub>21</sub>H<sub>21</sub>Br<sub>2</sub>P: C (54.34, 54.59), H (4.56, 4.70).

TPP-4C2B: <sup>1</sup>H NMR (400 MHz, CDCl<sub>3</sub>) δ (ppm): 7.87–7.70 (m, 9H), 7.69–7.55 (m, 6H), 3.86–3.66 (m, 2H), 3.48 (t, *J* = 6.1 Hz, 2H), 2.32–2.10 (m, 2H), 1.77 (dt, *J* = 15.4, 7.8 Hz, 2H), <sup>13</sup>C NMR (100 MHz, CDCl<sub>3</sub>) δ (ppm): 134.62, 134.59, 132.95, 132.85, 129.99, 129.87, 117.44, 116.58, 32.77, 32.57, 25.46, 21.14, 20.62, <sup>31</sup>P NMR (162 MHz, CDCl<sub>3</sub>) δ (ppm): 24.15, HRMS, *m/z*: ([M]<sup>+</sup>), calculated 397.0715, found, 397.0741, Elemental Analysis for C<sub>22</sub>H<sub>23</sub>Br<sub>2</sub>P: C (55.26, 55.66), H (4.85, 5.03).

## Supporting Information

Supporting Information is available from the Wiley Online Library or from the author.

## Acknowledgements

P.A. and N.L.C.L. contributed equally to this work. This work was financially supported by the National Science Foundation of China (No. 21788102), the Research Grants Council of Hong Kong (Nos. 16305618, 16305518, N-HKUST609/19, C6009-17G, and AoE/P-02/12), the Innovation and Technology Commission (No. ITC-CNERC14SC01), and the Science and Technology Plan of Shenzhen (No. JCYJ20160229205601482).

## Conflict of Interest

The authors declare no conflict of interest.

## Keywords

charge recombination, charge separation, charge transfer, organic long-persistent luminescence, phosphonium salts

Received: February 13, 2020

Revised: March 23, 2020

Published online:

- [1] W. M. Yen, M. J. Weber, *Inorganic Phosphors: Compositions, Preparation and Optical Properties*, CRC Press, Boca Raton, FL, USA **2004**.
- [2] J. Xu, S. Tanabe, *J. Lumin.* **2019**, *205*, 581.
- [3] Z. Li, Y. Zhang, X. Wu, L. Huang, D. Li, W. Fan, G. Han, *J. Am. Chem. Soc.* **2015**, *137*, 5304.
- [4] T. Maldiney, A. Bessière, J. Seguin, E. Teston, S. K. Sharma, B. Viana, A. J. J. Bos, P. Dorenbos, M. Bessodes, D. Gourier, D. Scherman, C. Richard, *Nat. Mater.* **2014**, *13*, 418.
- [5] H. Sun, L. Pan, X. Piao, Z. Sun, *J. Colloid Interface Sci.* **2014**, *416*, 81.
- [6] J. Wang, Q. Ma, W. Zheng, H. Liu, C. Yin, F. Wang, X. Chen, Q. Yuan, W. Tan, *ACS Nano* **2017**, *11*, 8185.
- [7] Q. le Masne de Chermont, C. Chanéac, J. Seguin, F. Pellé, S. Maîtrejean, J.-P. Jolivet, D. Gourier, M. Bessodes, D. Scherman, *Proc. Natl. Acad. Sci. USA* **2007**, *104*, 9266.
- [8] J. Liu, T. Lécuyer, J. Seguin, N. Mignet, D. Scherman, B. Viana, C. Richard, *Adv. Drug Delivery Rev.* **2019**, *138*, 193.
- [9] Z. Pan, Y.-Y. Lu, F. Liu, *Nat. Mater.* **2012**, *11*, 58.
- [10] K. Van den Eeckhout, P. F. Smet, D. Poelman, *Materials* **2010**, *3*, 2536.
- [11] Y. Li, M. Gecevicius, J. Qiu, *Chem. Soc. Rev.* **2016**, *45*, 2090.
- [12] S. Xu, R. Chen, C. Zheng, W. Huang, *Adv. Mater.* **2016**, *28*, 9920.
- [13] R. Kabe, C. Adachi, *Nature* **2017**, *550*, 384.
- [14] Z. Lin, R. Kabe, N. Nishimura, K. Jinnai, C. Adachi, *Adv. Mater.* **2018**, *30*, 1803713.
- [15] K. Jinnai, N. Nishimura, R. Kabe, C. Adachi, *Chem. Lett.* **2019**, *48*, 270.
- [16] K. Jinnai, R. Kabe, C. Adachi, *Adv. Mater.* **2018**, *30*, 1800365.
- [17] D. L. Wise, G. E. Wnek, D. J. Trantolo, T. M. Cooper, J. D. Gresser, *Photonic Polymer Systems: Fundamentals: Methods, and Applications*, CRC Press, Boca Raton, FL, USA **1998**.
- [18] Kenry, C. Chen, B. Liu, *Nat. Commun.* **2019**, *10*, 2111.
- [19] Y. Shoji, Y. Ikabata, Q. Wang, D. Nemoto, A. Sakamoto, N. Tanaka, J. Seino, H. Nakai, T. Fukushima, *J. Am. Chem. Soc.* **2017**, *139*, 2728.
- [20] W. Zhao, Z. He, J. W. Y. Lam, Q. Peng, H. Ma, Z. Shuai, G. Bai, J. Hao, B. Z. Tang, *Chem* **2016**, *1*, 592.
- [21] Y. Mu, Z. Yang, J. Chen, Z. Yang, W. Li, X. Tan, Z. Mao, T. Yu, J. Zhao, S. Zheng, S. Liu, Y. Zhang, Z. Chi, J. Xu, M. P. Aldred, *Chem. Sci.* **2018**, *9*, 3782.
- [22] Y. Tani, M. Terasaki, M. Komura, T. Ogawa, *J. Mater. Chem. C* **2019**, *7*, 11926.
- [23] G. W. Suter, A. J. Kallir, U. P. Wild, T. Vo-Dinh, *Anal. Chem.* **1987**, *59*, 1644.
- [24] J.-Q. Wang, Y. Mu, S.-D. Han, J. Pan, J.-H. Li, G.-M. Wang, *Inorg. Chem.* **2019**, *58*, 9476.
- [25] S. Hirata, *J. Mater. Chem. C* **2018**, *6*, 11785.
- [26] M. S. Kwon, D. Lee, S. Seo, J. Jung, J. Kim, *Angew. Chem., Int. Ed.* **2014**, *53*, 11177.
- [27] J. Wang, X. Gu, H. Ma, Q. Peng, X. Huang, X. Zheng, S. H. P. Sung, G. Shan, J. W. Y. Lam, Z. Shuai, B. Z. Tang, *Nat. Commun.* **2018**, *9*, 2963.
- [28] J. Yang, X. Gao, Z. Xie, Y. Gong, M. Fang, Q. Peng, Z. Chi, Z. Li, *Angew. Chem., Int. Ed.* **2017**, *56*, 15299.
- [29] H. Ma, A. Lv, L. Fu, S. Wang, Z. An, H. Shi, W. Huang, *Ann. Phys.* **2019**, *531*, 1800482.
- [30] S. Hirata, *Adv. Opt. Mater.* **2017**, *5*, 1700116.
- [31] S. Mukherjee, P. Thilagar, *Chem. Commun.* **2015**, *51*, 10988.
- [32] A. Forni, E. Lucenti, C. Botta, E. Cariati, *J. Mater. Chem. C* **2018**, *6*, 4603.
- [33] O. Bolton, K. Lee, H.-J. Kim, K. Y. Lin, J. Kim, *Nat. Chem.* **2011**, *3*, 205.
- [34] W. Z. Yuan, X. Y. Shen, H. Zhao, J. W. Y. Lam, L. Tang, P. Lu, C. Wang, Y. Liu, Z. Wang, Q. Zheng, J. Z. Sun, Y. Ma, B. Z. Tang, *J. Phys. Chem. C* **2010**, *114*, 6090.
- [35] X. Yang, D. Yan, *Adv. Opt. Mater.* **2016**, *4*, 897.
- [36] Z. An, C. Zheng, Y. Tao, R. Chen, H. Shi, T. Chen, Z. Wang, H. Li, R. Deng, X. Liu, W. Huang, *Nat. Mater.* **2015**, *14*, 685.
- [37] P. Data, Y. Takeda, *Chem. – Asian J.* **2019**, *14*, 1613.
- [38] H. Chen, X. Ma, S. Wu, H. Tian, *Angew. Chem., Int. Ed.* **2014**, *53*, 14149.
- [39] Z. Yang, Z. Mao, X. Zhang, D. Ou, Y. Mu, Y. Zhang, C. Zhao, S. Liu, Z. Chi, J. Xu, Y.-C. Wu, P.-Y. Lu, A. Lien, M. R. Bryce, *Angew. Chem., Int. Ed.* **2016**, *55*, 2181.
- [40] G. Zhang, G. M. Palmer, M. W. Dewhirst, C. L. Fraser, *Nat. Mater.* **2009**, *8*, 747.
- [41] G. Zhan, Z. Liu, Z. Bian, C. Huang, *Front. Chem.* **2019**, *7*, 305.
- [42] M.-M. Fang, J. Yang, Z. Li, *Chin. J. Polym. Sci.* **2019**, *37*, 383.
- [43] L. Xiao, H. Fu, *Chem. – Eur. J.* **2019**, *25*, 714.
- [44] N. Gan, H. Shi, Z. An, W. Huang, *Adv. Funct. Mater.* **2018**, *28*, 1802657.
- [45] M. Hayduk, S. Riebe, J. Voskuhl, *Chem. – Eur. J.* **2018**, *24*, 12221.
- [46] J. Karpiuk, A. Majka, E. Karolak, J. Nowacki, *J. Phys. Chem. Lett.* **2017**, *8*, 4659.
- [47] S. Kuno, H. Akeno, H. Ohtani, H. Yuasa, *Phys. Chem. Chem. Phys.* **2015**, *17*, 15989.
- [48] N. J. Turro, *Modern Molecular Photochemistry*, University Science Books, Sausalito, CA, USA **1991**.
- [49] S. Sumalekshmy, K. R. Gopidas, *Chem. Phys. Lett.* **2005**, *413*, 294.
- [50] W. H. Hamill, *J. Chem. Phys.* **1979**, *71*, 140.
- [51] A. Köhler, H. Bässler, *Electronic Processes in Organic Semiconductors*, Wiley-VCH, Weinheim, Germany **2015**, pp. 87–191.
- [52] T. T. Tidwell, in *Stable Radicals: Fundamentals and Applied Aspects of Odd-Electron Compounds* (Ed: R. G. Hicks), John Wiley & Sons, Chichester, UK **2010**, pp. 1–31.